International Journal of Mechanical, Industrial and Aerospace Sciences
ISSN: 2517-9950
Vol:5, No:2, 2011

Modeling of Bio Scaffolds: Structural and Fluid Transport Characterization

Sahba Sadir, M. R. A. Kadir, A. Öchsner , M. N. Harun

***Abstract*—**Scaffolds play a key role in tissue engineering and can be produced in many different ways depending on the applications and the materials used. Most researchers used an experimental trial-and- error approach into new biomaterials but computer simulation applied to tissue engineering can offer a more exhaustive approach to test and screen out biomaterials. This paper develops the model of scaffolds and Computational Fluid Dynamics that show the value of computer simulations in determining the influence of the geometrical scaffold parameter porosity, pore size and shape on the permeability of scaffolds, magnitude of velocity, drop pressure, shear stress distribution and level and the proper design of the geometry of the scaffold. This creates a need for more advanced studies that include aspects of dynamic conditions of a micro fluid passing through the scaffold were characterized for tissue engineering applications and differentiation of tissues within scaffolds.

***Keywords*—**Scaffold engineering, Tissue engineering, Cellular structure, Biomaterial, Computational fluid dynamics.

I. Introduction

SCAFFOLDS play a key role in tissue engineering and must meet different demands. The scaffold material has to be biodegradable and the products of degradation should be non-toxic. The scaffold structure has to be highly porous with a high interconnectivity and a surface area [1, 2, 3] which allows nutrient flow throughout the scaffold and the surrounding host tissue [4]. From a materials engineering point of view, tissues are considered to be cellular composites representing multiphase systems. Cellular composites are then seen as consisting of three main structural components: (1) cells organized into functional units, (2) the extracellular matrix and (3) scaffolding architecture. The design of a scaffold is necessary for its correct interaction with cells as indicated above. Moreover, it is essential that it fulfills its in vivo function. Biomaterials science has mainly adopted a 'trial-and-error' approach, with modifications being made to an existing design based on experimental in vitro or in vivo results. Improvements in cell culture conditions and the development of bioreactors have greatly improved the reliability of in vitro experiments. However, computer-aided design (CAD) can also contribute to the reduction of experimental tests and to shortening the design process of scaffolds [5, 6]. This technique can be used to design any kind of component or material and could be very useful for the design of scaffolds for tissue engineering; since a scaffold with different pore sizes or pore types can be modeled. Since mass and fluid transport are essential for providing the cells with the materials needed to differentiate, the natural tissue can provide information on the fluid and the flow conditions for a given cell type. Some studies have performed a computational fluid dynamics analyses within a scaffold. So far, only simulations of a perfusion bioreactor have been investigated [7, 8, 9]. In this study the effect of typical geometrical parameters, such as the porosity, the pore size and pore shape on the permeability of scaffolds, magnitude of velocity, drop pressure, shear stress distribution and level are investigated for tissue engineering application.

II. Methodology

Due to the high complexity of fluid dynamics, there is no other choice than to obtain the approximation solution numerically by the use of a CFD program. Powerful commercial CFD software, Fluent Inc. (2006) is utilized for analysis. The method used in such software is to discretize the fluid domain into small cells to form a volume mesh or grid, and then apply iterative methods to solve the equations of motion governed by the Navier-Stokes equations:

$$\rho(\mathrm{v}.\nabla\mathrm{v}) = -\nabla p + \mu\nabla^2\mathrm{v}. \tag{1}$$

where p and v are the pressure and velocity field respectively. The method devised in this work is to exports the cellular geometry, into the CFD software. The intrinsic permeability can be calculated using an empirical relationship known as Darcy's law. It relates the volumetric flow rate and induced pressure difference in a flow channel. Darcy's law for a viscous flow can be expressed as [6]:

$$K = \frac{\mu v}{\frac{\Delta \mathrm{p}}{\mathrm{L}}}. \tag{2}$$

Sahba Sadir is with Medical Implant Technology Group, Faculty of Mechanical Engineering, Universiti Teknologi Malaysia, Skudai, 81310, Johor, Malaysia (e-mail:sadir.sahba@gmail.com).

M. R. A. Kadir, is with Medical Implant Technology Group, Faculty of Biomedical Engineering and Health Sciences, Universiti Teknologi Malaysia, Skudai, 81310, Johor, Malaysia (phone: +607-5535961; fax: +607-5535430; e-mail: rafiq@biomedical.utm.my).

A. Öchsner is with the the Faculty of Mechanical Engineering, Universiti Teknologi Malaysia, Skudai, 81310, Johor, Malaysia (e-mail: andreas.oechsner@gmail.com).

M. N. Harun is with Medical Implant Technology Group, Faculty of Mechanical Engineering, Universiti Teknologi Malaysia, Skudai, 81310, Johor, Malaysia (e-mail: author@nrim.go.jp).

where K is the permeability coefficient, μ is the dynamic viscosity of the medium, L is the thickness, v is the fluid velocity and Δp is the pressure drop.

The cellular scaffolds (Fig.2) are placed inside a rectangular chamber (Fig. 1); the two planes of the chamber parallel cellular structure are the inlet pressure (velocity) and outlet pressure (velocity) boundaries. The four walls of the chamber are regarded as symmetry surfaces so that the results indicate a better depiction of real situations.

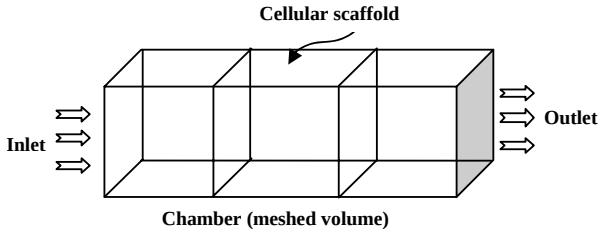

Fig. 1 Schematic of simulation set-up to find fluid-flow path.

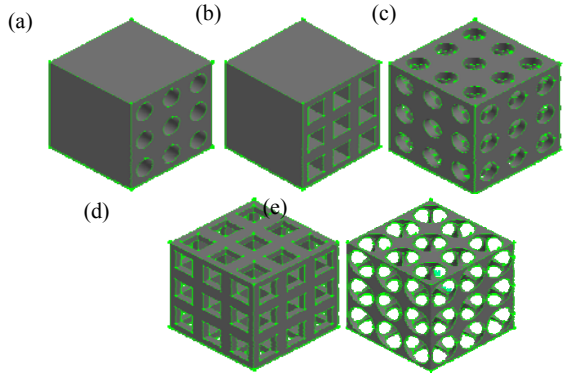

Fig. 2 (a) Cubic cellular structure with nine circular tube pores, (b) Cubic cellular structure with nine rectangular tube pores, (c) Cubic cellular structure with intersecting circular tubes in three dimensional, (d) Cubic cellular structure with intersecting rectangular tubes in three dimensional, (e) Cubic cellular structure with intersecting tubes with solid spheres(hollow sphere structure).

The CFD model was based on a simplification of the geometry of polymeric scaffolds. In the first step, cellular scaffolds are represented by the simplified model structure, using the cubic structure includes hollows cylinders with different diameters, then complex porous cell as can be seen in the Fig. 2.By varying the porosities of the cellular structures, a study is carried out to see how changes in porosities of the cellular structure affect the fluid flow.

A computer-Aided Design (CAD) package can be used for generating computational grids and some CFD software packages own their preprocessing tools like GAMBIT which is used in FLUENT. There are generally structured or unstructured girds that can be generated according to the geometry of flow domain defined. In structured girds, the grid cells lies in regular rows and columns. Cell shapes are dominated by quadrilaterals in two-dimensional solution domains or hexahedrons in three dimensional solution domains. In unstructured grids, cells are constructed in an irregular pattern. Triangular cells (2D) and tetrahedral cells, wedge cells or pyramid cells (3D) are employed in unstructured grids. The accuracy of a CFD solution is highly dependent upon the number of cells in its computational grid. In the preprocessing stage, the fluid properties and the conditions along the boundary of solution domain also need to be appropriately set.

Solid modeler Gambit (Fluent, Lebanon, NH, USA) was used to build the 3D model and the mesh. A 4-node tetrahedral mesh was used; the meshes presented a number of elements up to 200,000 depending on the porosity, with a corresponding number of nodes up to 50,000. No-slip boundary conditions were applied to the solid surfaces, under the hypothesis of rigid and impermeable walls. The fluid flows in from inlet and out from the outlet. A completely developed laminar flow was obtained at the inlet. The inlet velocity was $0.01\,\text{m/s}$. Liquid-water was used as the Newtonian fluid (a density of $\rho = 1000\,Kg/m^3$ and a viscosity $\vartheta = 0.001 kgm^{-1}s^{-1}$. Density and viscosity of the fluid were assumed to be constant, corresponding to the isothermal approach.

III. Result and Discussion

Fluid and mass transport rely on the fluid properties in the pore space and the geometry of the scaffold. The transport properties also rely on existing fluid velocities or pressures.

Steady-state Newtonian fluid analyses are performed with a non-slip condition on the walls of the scaffold. Fluid density and viscosity are similar to those of the cell culture medium. Fig. 3 shows respective maps of cross-sectional contour of velocity for all the models. High changes of fluid velocity are observed; there are regions where the fluid velocity is almost zero, and other parts with high-velocity fluid flow. Each pore of the samples had different values of fluid velocity, fluid pressure and fluid shear stress, depending mainly on its position within the scaffold, its size and its interconnectivity with other pores. It can be from Figs. 4, 6, 8, 10 and 12, porosity and size of pore affect on drop pressure. For the same pore size with decreasing porosities, drop pressure increase, and for the constant porosity with reducing pore size drop pressure is increased. Figs. 5, 7, 9, 11 and 13 outlines the calculated wall shear-stress distribution measured for all models. It can be seen the pore size and shape affects the shear stress level and distribution, while the porosity affects only the distribution. So the simulations showed that the pore size is a variable strongly influencing the predicted shear stress level, whereas the porosity is a variable strongly affecting the statistical distribution of the shear stresses but not their mode value, for a given pore geometries.

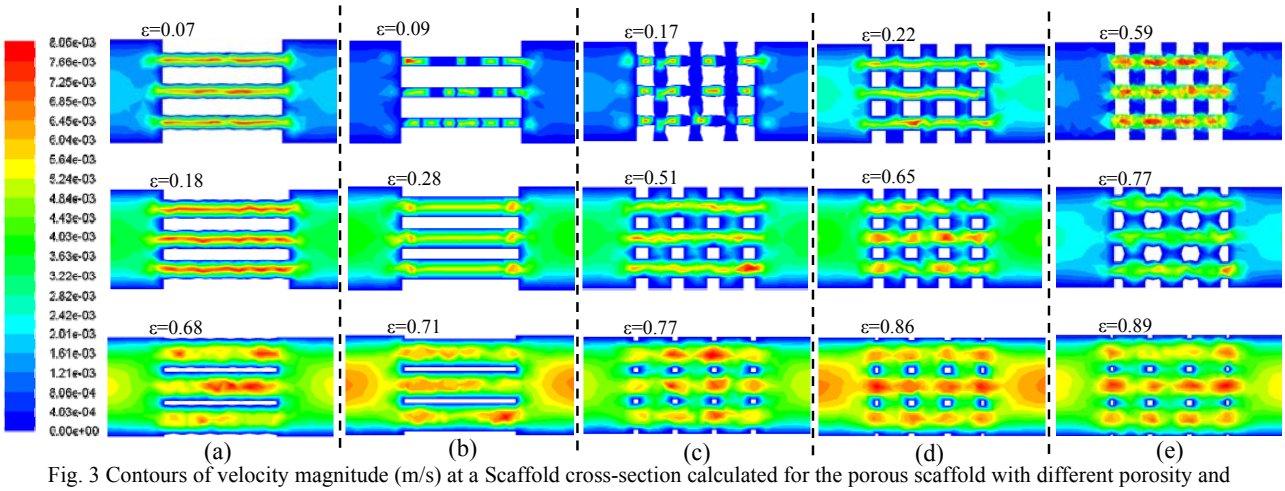

Fig. 3 Contours of velocity magnitude (m/s) at a Scaffold cross-section calculated for the porous scaffold with different porosity and configuration (a) Cubic cellular structure with nine circular tube pores, (b) Cubic cellular structure with nine rectangular tube pores, (c) Cubic cellular structure with intersecting circular tubes in three dimensional, (d) Cubic cellular structure with intersecting rectangular tubes in three dimensional, (e) Cubic cellular structure with hollow sphere structure.

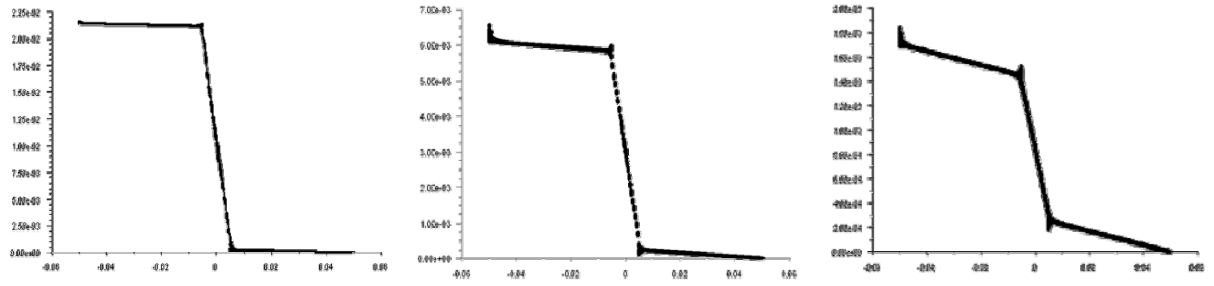

Fig. 4 Pressure drop through cellular structure for Cubic cellular structure with nine circular tube pores with three different porosities (a) ε= 0.07, (b) ε = 0.18 (c) ε = 0.68. (Pressure Vs. Position)

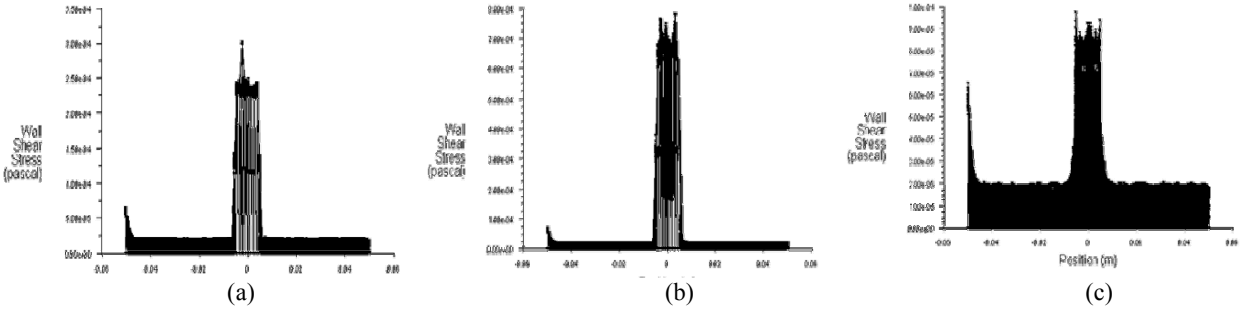

Fig. 5 Wall shear stress distribution through cellular structure for Cubic cellular structure with nine circular tube pores with three different porosities (a) ε= 0.07, (b) ε = 0.18 (c) ε = 0.68. (Wall shear stress Vs. Position)

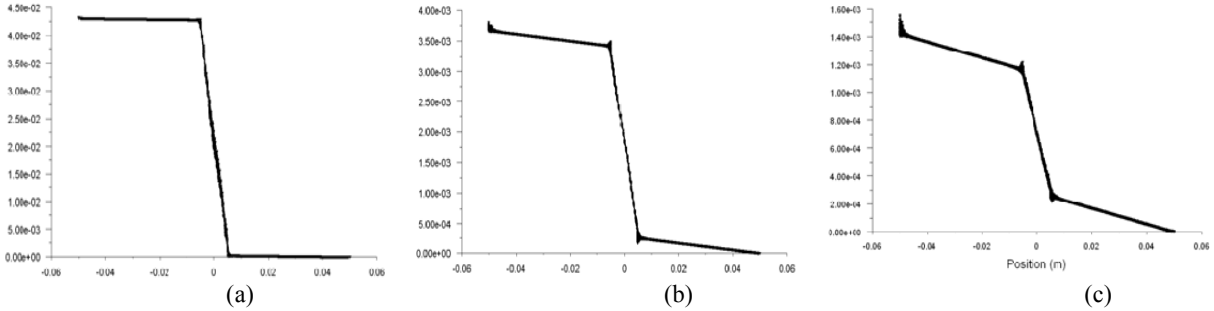

Fig. 6 Pressure drop through cellular structure for Cubic cellular structure with nine rectangular tube pores with three different porosities (a) ε= 0.09, (b) ε = 0.28 (c) ε = 0.71. (Pressure Vs. Position)

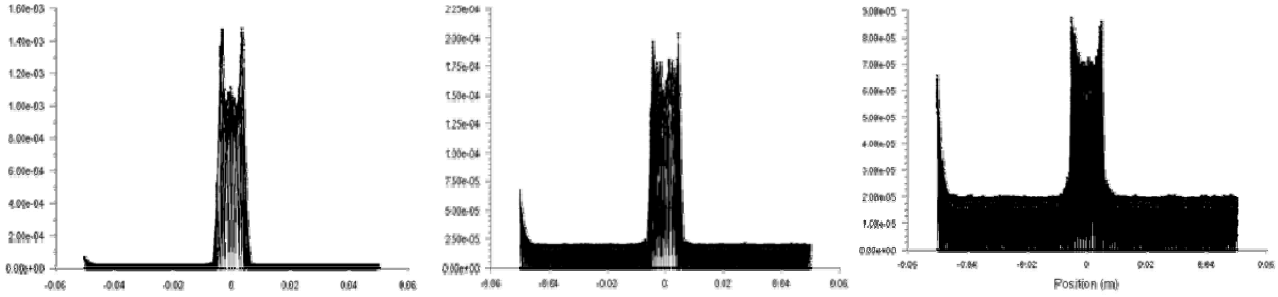

(a) (b) (c)

Fig. 7 Wall shear stress distribution through cellular structure for Cubic cellular structure with nine rectangular tube pores with three different porosities (a) ε= 0.09, (b) ε = 0.28 (c) ε = 0.71 (Wall shear stress Vs. Position)

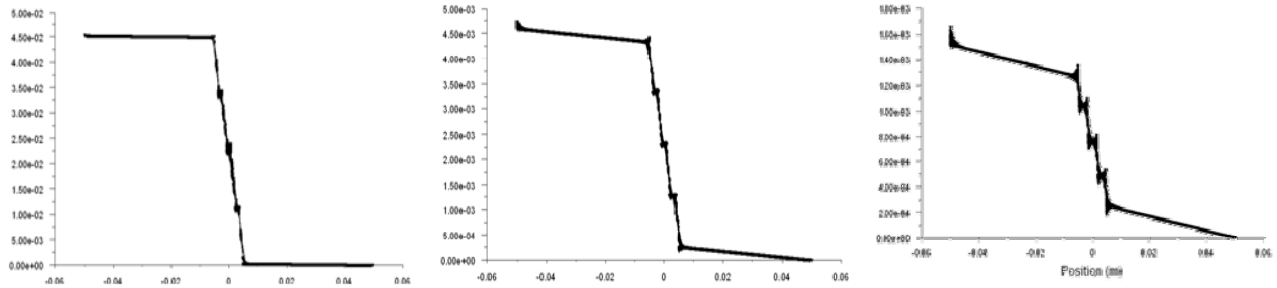

(a) (b) (c)

Fig. 8 Pressure drop through cellular structure for Cubic cellular structure with intersecting circular tubes with three different porosities (a) ε= 0.17, (b) ε = 0.51 (c) ε = 0.77 (Pressure Vs. Position)

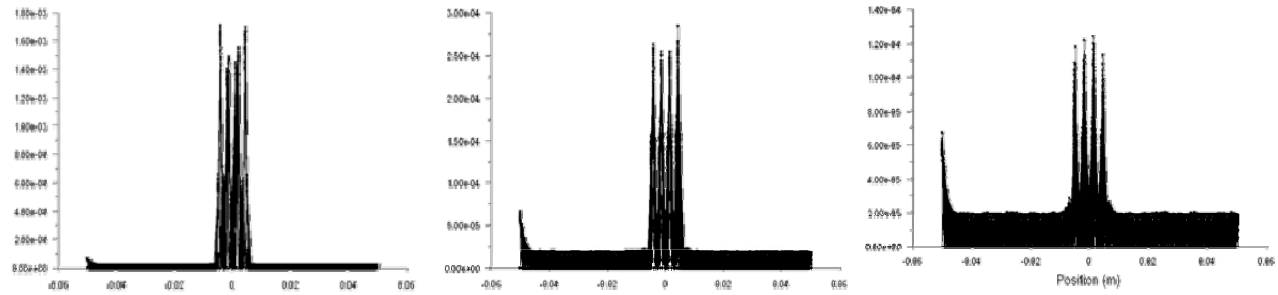

(a) (b) (c)

Fig. 9 Wall shear stress distribution through cellular structure for Cubic cellular structure with intersecting circular tubes with three different porosities (a) ε= 0.17, (b) ε = 0.51 (c) ε = 0.77 (Wall shear stress Vs. Position)

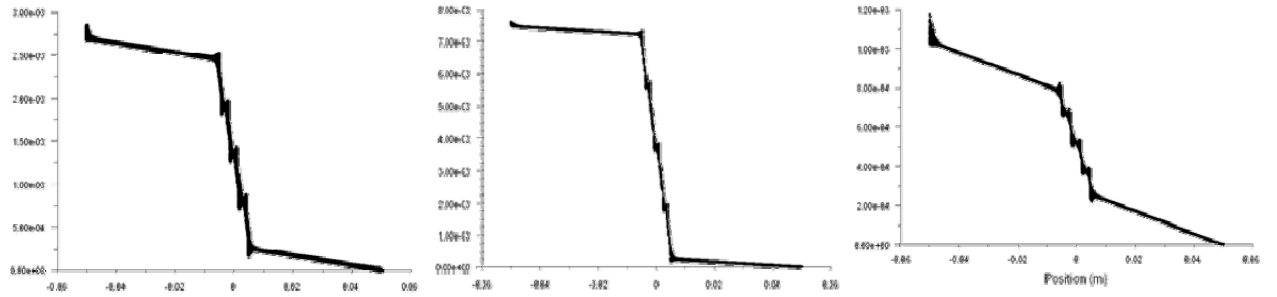

(a) (b) (c)

Fig. 10 Pressure drop through cellular structure for Cubic cellular structure with intersecting rectangular tubes with three different porosities (a) ε= 0.22, (b) ε = 0.65 (c) ε = 0.86 (Pressure Vs. Position)

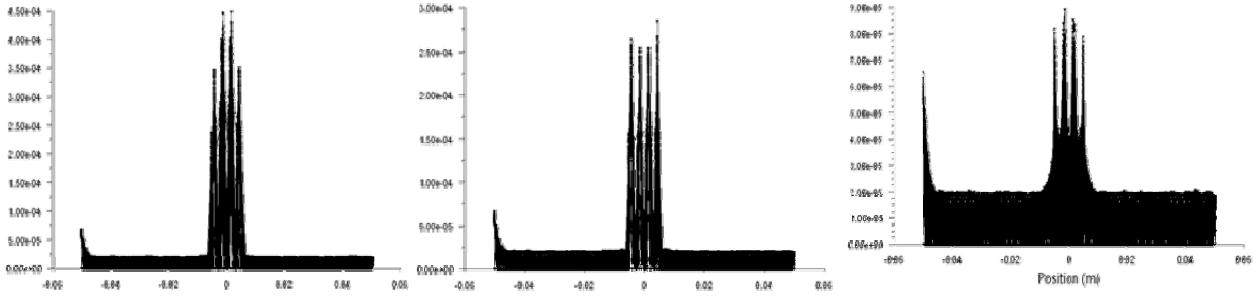

(a) (b) (c)

Fig. 11 Wall shear stress distribution through cellular structure for Cubic cellular structure with intersecting rectangular tubes with three different porosities (a) ε= 0.22, (b) ε = 0.65 (c) ε = 0.86 (Wall shear stress Vs. Position)

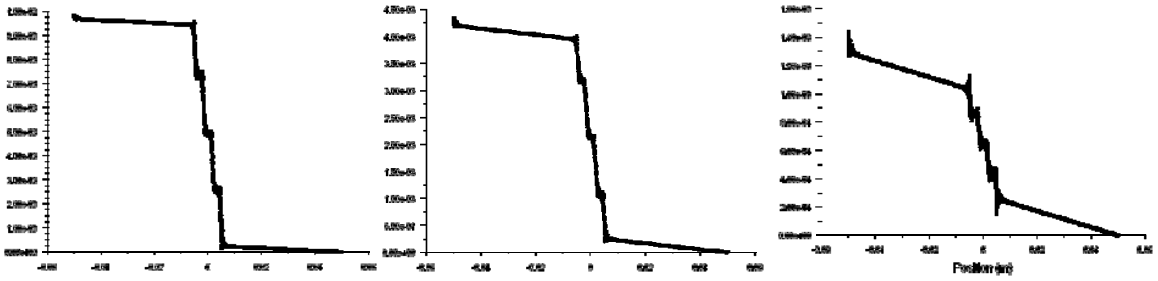

(a) (b) (c)

Fig. 12 Pressure drop through cellular structure for Cubic cellular structure with hollow sphere structure with three different porosities (a) ε= 0.59, (b) ε = 0.77 (c) ε = 0.89 (Pressure Vs. Position)

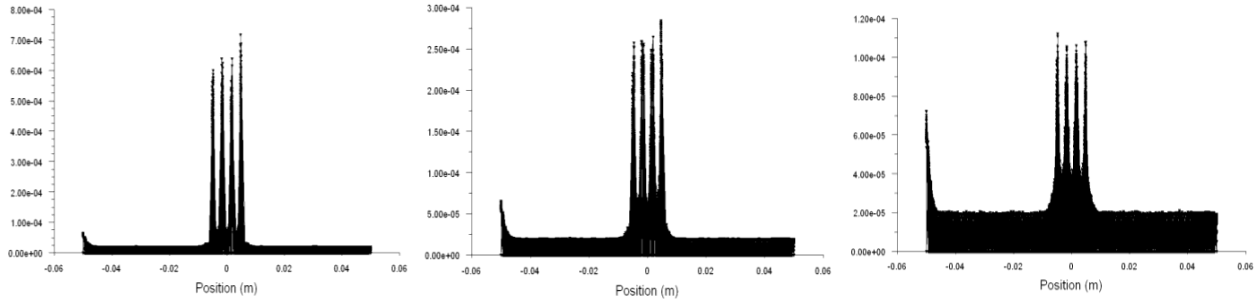

(a) (b) (c)

Fig. 13 Wall shear stress distribution through cellular structure for Cubic cellular structure with hollow sphere structure with three different porosities (a) ε= 0.59, (b) ε = 0.77 (c) ε = 0.89 (wall shear stress Vs. Position)

According to the Darcy's law (2), the permeability values shown in Table 1 for several types of scaffolds and different size and shape of pore are acquired on the basis of Darcy equation

TABLE I
POROSITIES AND PERMEABILITY VALUES FOR CONSIDERED MATRICES

Type Matrix	Porosity m^3/m^3	Permeability m^2
Cubic cellular structure with nine tube cylinder pores	0.07	2.37×10^{-6}
	0.18	5.81×10^{-6}
	0.68	1.13×10^{-5}
Cubic cellular structure with nine rectangular tube pores	0.09	2.77×10^{-6}
	0.28	8.65×10^{-6}
	0.71	1.23×10^{-5}
Cubic cellular structure with intersecting circular tubes in 3D	0.17	3.57×10^{-6}
	0.51	8.34×10^{-6}
	0.77	1.31×10^{-5}
Cubic cellular structure with intersecting rectangular tubes in 3D	0.22	7.96×10^{-6}
	0.65	1.08×10^{-5}
	0.86	2.05×10^{-5}
Cubic cellular structure with intersecting circular tubes in 3D	0.59	8.87×10^{-6}
	0.77	1.31×10^{-5}
	0.89	2.12×10^{-5}

A possible explanation for the discrepancy between this study and pervious studies is that the scaffold dimensions, and architecture are vastly different, these parameters can be expected to influence the properties of fluid flow through the

scaffolds. Furthermore, biomaterial interactions due to local surface chemistry and morphology may affect the response of cells to specific shear stress regimes; thus, simply reporting flow rates does not allow direct comparisons between perfusion studies; however, in this paper, the application of the computational fluid dynamics described here provides a practical means for such comparisons and surely be useful for designing perfusion systems and scaffold microarchitectures to develop of 3-D tissue constructs.

IV. Conclusion

In the presented study, a considerably different fluid dynamic behavior was estimated by using of microscopic cellular scaffolds. The usage of a simplified geometry with a regular and homogeneous distribution of pores allowed us to study the effect of typical geometrical parameters, such as the porosity, size and configuration of the pores on the magnitude of velocity, drop pressure and shear stress distribution and level. Each pore of the samples had different values of fluid velocity, fluid pressure and fluid shear stress, depending mainly on its position within the scaffold, its size and its interconnectivity with other pores; as result it was obvious that by decreasing porosities, drop pressure increased, and for the constant porosity with reducing pore size drop pressure is increased; indeed, pore size and shape affects the shear stress level and distribution, whereas the porosity affects only on its distribution; therefore, the simulations showed that the pore size is a variable strongly influencing the predicted shear stress level. The presented results can be useful for designing perfusion systems and scaffold microarchitectures to develop of 3-D tissue constructs.

Acknowledgment

This project was supported by Bio-TEG research center, Universiti Teknologi Malaysia. The authors would also like to thank the Research Management Centre, Universiti Teknologi Malaysia.

References

[1] A. G. Mikos and J. S. Temenoff, Formation of highly porous biodegradable scaffolds for tissue engineering, EJB Electronic Journal of Biotechnology 3(2): 1-6, 2000.

[2] Freed, L.E., Vunjac-Novakovic, G., “Tissue engineering of cartilage”, In: Bronzino, J.D. (Ed.), The Biomedical Engineering Handbook. CRC Press, Boca Raton, FL, pp. 1788–1806, 1995

[3] Freed, L.E., Langer, R., Martin, I., Pellis, N.R., Vunjak-Novakovic, G., “Tissue engineering of cartilage in space”, Proceedings of the National Academy of Sciences USA 94 (25), pp. 1385–1390, 1997

[4] Kellner, K., Liebsch, G., Klimant, I., Wolfbeis, O.S., Blunk, T., Schulz, M.B., Gopferich, A., “Determination of oxygen gradients in engineered tissue using a fluorescent sensor”, Biotechnology and Bioengineering 80 (1), pp. 73–83, 2002

[5] Sun, W. & Lal, P., Recent development on computer aided tissue engineering—a review, Comput. Methods Prog. Biomed. 67, 85–103. 2002

[6] Sun, W., Darling, A., Starly, B. & Nam, J., Computer aided tissue engineering: overview, scope and challenges, J. Biotechnol. Appl. Biomech. 39, 29–47, 2004.

[7] Cioffi, M., Boschetti, F., Raimondi, M. T. & Dubini, G., Modeling evaluation of the fluid dynamic microenvironment in tissue-engineered constructs: a micro-CT based model, Biotechnol. Bioeng. 93, 500–510, 2006.

[8] Boschetti F, Raimondi MT, Migliavacca F, Dubini G, “Prediction of the micro-fluid dynamic environment imposed to three-dimensional engineered cell systems in bioreactors”, Journal Biomechanics 39(3), pp. 418–425. 2006.

[9] Sandino, C., Planell, J. A. & Lacroix, D., A finite element study of mechanical stimuli in scaffolds for bone tissue engineering, J. Biomech. 41, 1005–1014, 2008

[10] Scheidegger A E, “The Physics of Flow through Porous Media” (Toronto, Canada: University of Toronto Press), 1974.